

Energy Bands for the (001) Surface of Aluminum*

Ed Caruthers, Leonard Kleinman, and Gerald P. Alldredge

Department of Physics, University of Texas, Austin, Texas 78712

(Received 30 May 1973)

An energy-band calculation has been performed on a 13-layer film of (001) aluminum. Surface states are found at $\bar{\Gamma}$, \bar{M} , and \bar{X} in the two-dimensional Brillouin zone, and along the lines connecting these points. Wave functions are plotted and decay constants tabulated for some of these surface states. The charge density in the [001] direction has also been plotted for various positions in the planar unit cell, and for an average over the unit cell. Finally, the 13-layer energy bands are compared to a (001) projection of the three-dimensional energy bands, and effects of film thickness as well as the surface perturbation are shown.

INTRODUCTION

A new method of performing band calculations on thin films has recently been developed¹ and applied to lithium. Since the surface states found in lithium lie above the Fermi energy, and are not easily verified experimentally, interest turned to other simple metals where there was some indication of occupied surface states. A calculation by Boudreaux² indicated that there should be states below the Fermi energy localized on the (001) and (111) surfaces of aluminum. Our preliminary investigation indicated that there should be surface states at $\bar{\Gamma}$, \bar{M} , and \bar{X} on the (001) face, though Boudreaux reported no surface state at \bar{X} . It also seemed that the constant-width band gap which Boudreaux shows extending all the way from $\bar{\Gamma}$ to \bar{M} is impossible. Because of this, a new calculation of the energy bands of (001) Al has been performed. In the course of analyzing our results we have found that aluminum is a particularly nice material in which to show the ways in which film thickness and the intrinsic properties of a surface affect bulk energy bands.

II. PRELIMINARY INVESTIGATIONS

It is possible to find the general features of the thin-film energy bands by projecting the three-dimensional bands onto a two-dimensional surface. The actual bands for a thin film will differ from the projection because of the presence of surfaces, and because of the finite thickness of the film. By comparing the projection with bands for films of various thicknesses, it is possible to infer the band structure of very thick films or semi-infinite crystals. Completely surface-localized electronic surface states can exist only within energy gaps in the two-dimensional projection. This method has been used for the surface-phonon problem³ but as far as we know the method has never previously been applied to electronic levels at a surface.

To perform this projection it is necessary to calculate the three-dimensional eigenvalues along

the lines of high symmetry in the two-dimensional Brillouin zone, and at points above (i. e., in the [001] direction from) these symmetry lines. We have done this with a local-pseudopotential calculation, starting with the tabulated Heine-Animalu (H-A) potential.⁴ This gives good agreement with the values of the two matrix elements which Ashcroft⁵ derived from the de Haas-van Alphen data, as shown in Table I.

Heine and Animalu obtained their atomic pseudopotential by screening an ionic pseudopotential with the dielectric function. Because linear response theory is not valid for the very strong ionic V_0 , their atomic V_0 is expected to be incorrect. In fact, they obtain $V_0 = -0.5736$ Ry which leads to a negative work function. We chose V_0 to be -1.17 Ry, the value Lang and Kohn⁶ find for the potential in the interior of jellium with the electronic density of aluminum and which leads to fair agreement with the experimental work function. We joined the H-A pseudopotential at $k=0.8k_F$ to a smooth curve going to -1.17 Ry at $k=0$. Because $0.8k_F$ is much smaller than the smallest reciprocal-lattice vector (in two or three dimensions) this has no effect on the bulk energy bands other than to shift them uniformly. For improved convergence we multiplied the H-A pseudopotential by the Fermi-like function $(1 + e^{(k-k_c)/\Delta})^{-1}$, where $k_c = 10.5a_0^{-1}$ and $\Delta = 1.45a_0^{-1}$ with a_0 the Bohr radius. This is more reasonable than the common practice^{2,7} of assuring convergence by taking only V_{111} and V_{200} to be nonzero.

In Fig. 1 we show a (001) projection of the fcc lattice. The two-dimensional square unit cell is

TABLE I. Comparison of the Heine-Animalu local pseudopotential to Ashcroft's results.

	V_{111}	V_{200}
Ashcroft	0.0179 Ry	0.0562 Ry
Heine-Animalu	0.0147 Ry	0.0581 Ry

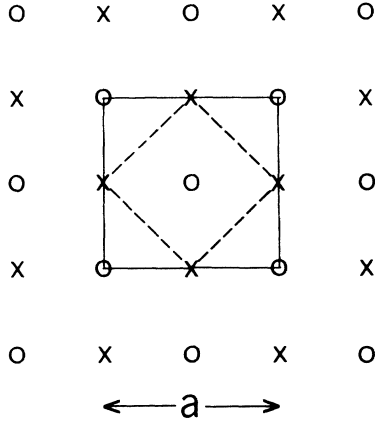


FIG. 1. (001) projection of the fcc lattice. The dashed line represents the base of the commensurate unit cell.

seen to be rotated 45° in the xy plane with respect to the three-dimensional crystal axes and the sides to be of length $\bar{a} = a/\sqrt{2}$. The three-dimensional unit cell commensurate with the two-dimensional cell is then defined by the lattice vectors $a(0, 0, 1)$, $a(\frac{1}{2}, \frac{1}{2}, 0)$, and $a(\frac{1}{2}, -\frac{1}{2}, 0)$ and the commensurate reciprocal-lattice vectors are $(2\pi/a)(0, 0, 1)$, $(2\pi/a)(1, 1, 0)$, and $(2\pi/a)(1, -1, 0)$.

In Fig. 2 we show the energy bands of the three-dimensional crystal projected onto the two-dimensional (001) Brillouin zone. Along $\bar{\Delta}$, i. e., $\bar{k} = (2\pi/\bar{a})(\alpha, 0)$, we have $\bar{k} = (2\pi/a)(\alpha, \alpha, \zeta)$ with $0 \leq \alpha \leq \frac{1}{2}$ and $0 \leq \zeta \leq 1$. (Note that unitalicized Roman letters with over bar denote two-dimensional vectors.³) We have plotted the bands as a function of α for fixed values of ζ differing by intervals of 0.1. Note that at \bar{X} , i. e., $\alpha = \frac{1}{2}$, the $(\frac{1}{2}, \frac{1}{2}, \zeta)$ and $(\frac{1}{2}, \frac{1}{2}, 1 - \zeta)$ states are degenerate except for ζ exactly equal to 0.5.⁸ This is because although $-(\frac{1}{2}, \frac{1}{2}, 1 - \zeta)$ is a different point than $(\frac{1}{2}, \frac{1}{2}, \zeta)$ in the commensurate Brillouin zone, it differs from it by a $(1, 1, 1)$ reciprocal-lattice vector and therefore comes from an equivalent point in the primitive three-dimensional Brillouin zone. Lines which differ in ζ have different three-dimensional \bar{k} vectors and therefore may cross on another (although in a finite slab where the three-dimensional symmetry is broken, they will not). Because all negative energy levels at $\bar{\Delta}$ have the same $\bar{\Delta}_1$ symmetry, lines with the same ζ values must repel one another. This causes gaps in the two-dimensional energy bands. There are two such gaps in the negative energy range at $\bar{\Delta}$. The upper gap starts at \bar{X} but is quickly pinched off as bands of different ζ (0 from the lower edge and 1.0 from the upper edge) cross each other. The lower gap persists all the way from \bar{X} to $\bar{\Gamma}$ at the locus of points for which bands with the same ζ values meet and repel each other with ζ going from 0.5 at \bar{X} to 1.0

at a point about midway across the band and remaining at 1.0 from that point over to $\bar{\Gamma}$. The gap at $\bar{\Gamma}$ is caused by V_{200} , being mainly due to the interaction of $(0, 0, 1)$ and $(0, 0, -1)$ plane waves. Similarly the upper \bar{X} gap is caused by V_{200} interacting between $(\frac{1}{2}, \frac{1}{2}, 1)$ and $(\frac{1}{2}, \frac{1}{2}, -1)$ plane waves. In fact, if higher $\zeta = 1$ bands did not come down to repel the two lowest $\zeta = 1$ bands, this gap would persist continuously from $\bar{\Gamma}$ to \bar{X} . The lower \bar{X} gap which actually does persist over to the $\bar{\Gamma}$ gap is mainly due to V_{111} acting between $(\frac{1}{2}, \frac{1}{2}, \frac{1}{2})$ and $(-\frac{1}{2}, -\frac{1}{2}, -\frac{1}{2})$ plane waves. The lower \bar{X} gap is much smaller than the other two gaps because V_{111} is much smaller than V_{200} .

Along \bar{Y} where $\bar{k} = (2\pi/\bar{a})(\frac{1}{2}, \alpha)$ and $\bar{k} = (2\pi/a) \times (\frac{1}{2} + \alpha, \frac{1}{2} - \alpha, \zeta)$ again with $0 \leq \alpha \leq \frac{1}{2}$ and $0 \leq \zeta \leq 1$, the twofold degeneracy between states with ζ and $1 - \zeta$ is maintained. Each degenerate pair consists of states of \bar{Y}_1 and \bar{Y}_2 symmetry. Thus here again we cannot have states with the same ζ crossing one another. The gap between states with $\zeta = 0.5$ goes continuously from \bar{X} to \bar{M} getting progressively narrower and vanishing at the \bar{M} point. [The \bar{M} point where the two $\zeta = 0.5$ states become degenerate comes from the twofold degenerate level at $W = (1, 0, \frac{1}{2})$ in three dimensions.⁵] However, this gap between $\zeta = 0.5$ levels is an absolute gap only about 88% of the distance from \bar{X} to \bar{M} ; at that point it is crossed by a $\zeta = 1.0$ and $\zeta = 0$ degenerate pair and from there over to \bar{M} by a continuum of states with different ζ values. The upper gap extending from \bar{X} to \bar{M} is similar to the gap extending from $\bar{\Gamma}$ to \bar{X} except that it is pinched off at \bar{M} . This occurs because the $\zeta, 1 - \zeta$ degeneracies at \bar{M} can have the twofold-degenerate \bar{M}_5 symmetry or can consist of \bar{M}_1 and \bar{M}_4 states whose degeneracy is due to the three-dimensional symmetry and does not persist in the two-dimensional thin film. Because they have different symmetries the \bar{M}_5 states can be degenerate with \bar{M}_1 \bar{M}_4 states with the same ζ value; this occurs for the $\zeta = 0.425, \zeta = 0.575$ pair, pinching off the gap. A continuum of \bar{M}_5 states exist from the lowest $\zeta = 0, \zeta = 1$ point at \bar{M} up to the positive energy range whereas the \bar{M}_1 \bar{M}_4 states start at the second $\zeta = 0, \zeta = 1$ point and continue only to the second $\zeta = 0.5$ point where a gap appears. They then exist from the third $\zeta = 0.5$ point continuously into the positive energy range.⁹ The range of \bar{M}_1 \bar{M}_4 states is indicated in Fig. 2 by vertical bars. Within this gap \bar{M}_1 or \bar{M}_4 surface states may occur but as soon as one goes away from \bar{M} by an infinitesimal $\delta\bar{k}$ in any direction these states will have the same symmetry as some of the states with which they are degenerate and will therefore be surface resonances rather than truly localized surface states.

We next consider the states along $\bar{\Sigma}$ where $\bar{k} = (2\pi/\bar{a})(\alpha, \alpha)$ and $\bar{k} = (2\pi/a)(2\alpha, 0, \zeta)$ again with

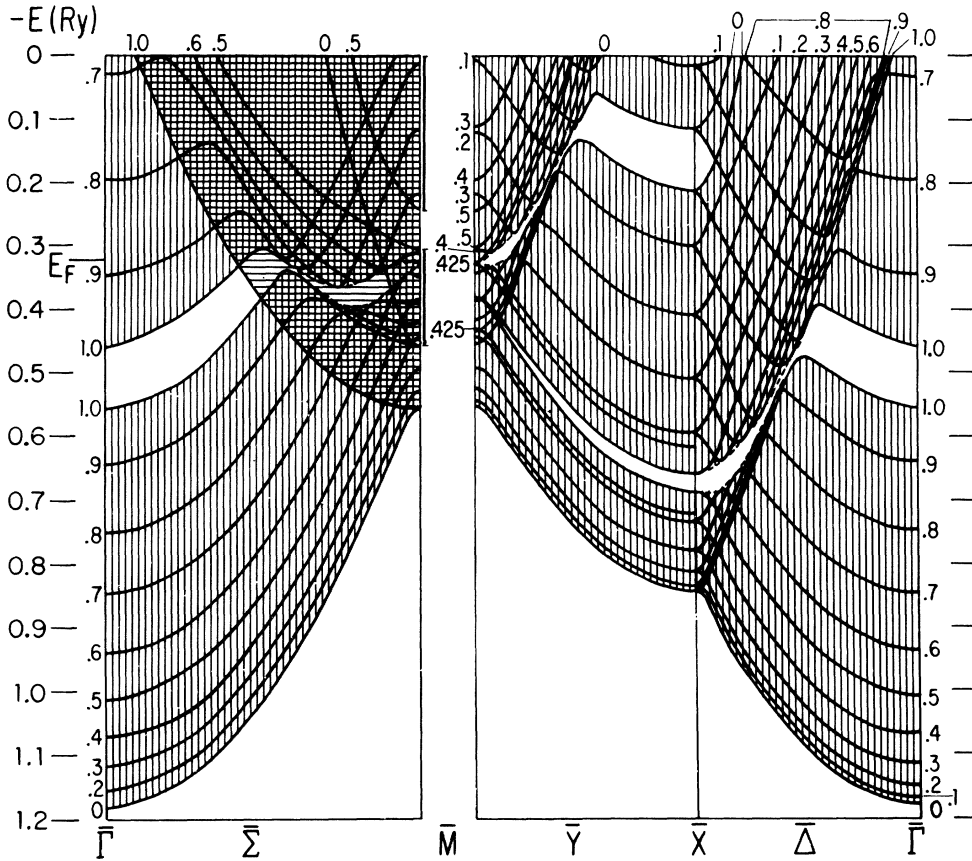


FIG. 2. Two-dimensional (001) projection of the three-dimensional energy bands of aluminum. The horizontal and vertical crosshatching represent continua of states with different symmetries. The numbers labeling the various bands represent values of k_z in units of $2\pi/a$.

$0 \leq \alpha \leq \frac{1}{2}$ and $0 \leq \zeta \leq 1$. All the negative energy $\bar{\Gamma}$ states have $\bar{\Gamma}_1$ symmetry and these are compatible with $\bar{\Sigma}_1$ states. At \bar{M} the \bar{M}_1 and \bar{M}_4 states are compatible with $\bar{\Sigma}_1$ whereas \bar{M}_5 is compatible with both $\bar{\Sigma}_1$ and $\bar{\Sigma}_2$. For the sake of clarity we only show a few of the bands in Fig. 2 which sweep upward in energy away from \bar{M} . The gap at $\bar{\Gamma}$ continues between $\zeta=1$ states until just past half-way to \bar{M} , then it becomes a locus of repelling bands with ζ decreasing continuously to 0.575 at \bar{M} where the gap is pinched off just as is the \bar{Y} gap at the same point. The bottom of the gap is crossed exactly half-way between $\bar{\Gamma}$ and \bar{M} , i. e., at $\alpha=0.25$, by another $\zeta=1$ state but with $\bar{\Sigma}_2$ symmetry. This crossing point comes from the twofold-degenerate level at $W=(\frac{1}{2}, 0, 1)$ in three dimensions. To the right of this $\bar{\Sigma}_2$ band the gap is filled by a continuum of $\bar{\Sigma}_2$ bands but still remains a $\bar{\Sigma}_1$ gap capable of containing a $\bar{\Sigma}_1$ surface state. Although the gap in $\bar{\Sigma}_1$ states emanating from negative energy $\bar{\Gamma}_1$ states persists all the way to \bar{M} , at a point about 90% of the way over toward \bar{M} a continuum of $\bar{\Sigma}_1$ bands (beginning with a $\zeta=0$ band) sweeping up-

ward from \bar{M} toward positive energy $\bar{\Gamma}$'s crosses the gap, and therefore in this region the gap can contain no surface states of any symmetry. Note that our gap is in no way similar to that of Boudreaux² which extends with almost constant width all the way from $\bar{\Gamma}$ to \bar{M} . The $\bar{\Sigma}$ surface states which he finds near \bar{M} cannot exist according to our picture, and in fact the motivation for our making this projection was that we did not find such surface states in the thin-film calculation discussed in Sec. III. We were able to generate a gap similar to Boudreaux's by considering only \bar{k} vectors within the primitive three-dimensional Brillouin zone with the planar projection of \bar{k} equal to \bar{k} in two dimensions.¹⁰ We suspect that Boudreaux's gap may have resulted from this error, but we do not understand how he could have found surface states in such a "gap." (See Note added in proof.)

III. THIN-FILM CALCULATIONS

In deriving a thin-film potential from the three-dimensional potential some care must be taken. The common procedure¹¹ is to use an unperturbed

crystal potential right through the last occupied layer of the film, and then to jump discontinuously to a uniform vacuum potential. But even though this model simplifies analysis, the potential is clearly unphysical. A more reasonable potential results from overlapping atomic potentials (or pseudopotentials). This gives a potential which falls off smoothly over a few interplanar spacings. However, experience with a self-consistent calculation¹² shows that such a potential falls off too rapidly in the selvage region and builds up a little too much charge at the center of the film. The correct falloff of the potential is probably that found by Lang and Kohn⁶ in their jellium calculation.

As we have done previously,¹ we took our 13-layer thin film to have a unit cell $\bar{a} \times \bar{a} \times 2L$ where $2L = 19a/2$, i. e., thirteen planes of atoms separated by $\frac{1}{2}a$ and three empty planes on each side forming the selvage regions in which the wave functions decay to zero. The complete set of basis functions obeying the two-dimensional periodic boundary conditions and vanishing at $(x, y, \pm L)$ is

$$\begin{aligned} \varphi_{\bar{\alpha},n}(\bar{k}) &= 2^{1/2} e^{i(\bar{k} \cdot \bar{\alpha})} \cdot \bar{r} \sin n\pi z/2L, \\ &\quad n \text{ an even integer} \\ &= 2^{1/2} e^{i(\bar{k} \cdot \bar{\alpha})} \cdot \bar{r} \cos n\pi z/2L, \\ &\quad n \text{ an odd integer} \end{aligned} \quad (1)$$

where \bar{k} is a k vector within the two-dimensional Brillouin zone and $\bar{\alpha}$ is a two-dimensional reciprocal-lattice vector. Using our previous method¹ for obtaining the thin-film potential we superpose H-A atomic pseudopotentials (modified for very small and very large \bar{k} as discussed in Sec. II) to get

$$V_{\text{film}}(\bar{G}, k_z) = S(\bar{G}, k_z) V_{\text{HA}}(\bar{G}, k_z) / N, \quad (2)$$

where N is the total number of layers in the film including selvage, $S(\bar{G}, k_z)$ is the structure factor obtained by summing over the 13 atomic positions in the 19-layer unit cell, and $k_z = n\pi/L$. For large \bar{k} vectors there is no reason to expect this potential to be unsatisfactory and therefore we use it for all $\bar{G} \neq 0$. For small \bar{k} vector corresponding to large values of \bar{r} , a superposition of atomic pseudopotentials is not good even if modified to have the correct V_0 . For bulk calculations this causes no problems aside from a constant shift of all the bands due to uncertainties in V_0 . The superposition of atomic potentials contains errors of two sorts. The tails of the atomic charge distributions are greatly modified when the atom is in a crystal, affecting small- \bar{k} Fourier transforms. Even more important is the problem of exchange. The potential in the selvage region of jellium is known⁶ to rise to its vacuum value very slowly. This is due

almost entirely to exchange and correlation. The cube root of the charge density appearing in the Kohn-Sham exchange approximation greatly enhances the value of the exchange when the charge density is small. One could probably obtain a fairly good potential in the selvage region by including exchange in the H-A atomic pseudopotential but this would cause one to superpose the cube roots of the atomic charge densities in the interior of the film rather than to take the cube root of the superposed charge densities. This leads to disaster; e. g., in lithium¹ one obtains a work function too large by an order of magnitude. Because the H-A pseudopotential seems to lead to satisfactory results in bulk calculations without the specific inclusion of an exchange term, we constructed $V_{\text{film}}(0, k_z)$ in the following manner. We start with $V_{\text{bulk}}(0, k_z)$ obtained from a superposition of H-A atomic pseudopotentials; we then Fourier transform back to obtain $V_{\text{bulk}}(0, z)$ which is the bulk potential averaged over the z plane as a function of z . We then take

$$\begin{aligned} V_{\text{film}}(0, z) &= V_{\text{bulk}}(0, z) V_j(z) / V_j(0) \\ &\quad \text{for } |z| < |z_c|, \\ V_{\text{film}}(0, z) &= V_j(z) \text{ for } |z| > |z_c|, \end{aligned} \quad (3)$$

where $V_j(z)$ is the Lang-Kohn⁶ jellium potential, $V_j(0) = -1.17$ Ry is their bulk value of the jellium potential and z_c is the largest value of z for which the bulk and jellium potentials cross. In Fig. 3 we show $V_{\text{film}}(0, z)$ and $V_j(z)$; the discontinuous derivative of $V_{\text{film}}(0, z_c)$ has been smoothed out. This potential is obviously quite good for either $|z| \gg |z_c|$ or $|z| \ll |z_c|$ and is probably as good as can be obtained for $|z| \approx |z_c|$ without a fully self-consistent calculation. Finally, to obtain V_{film}

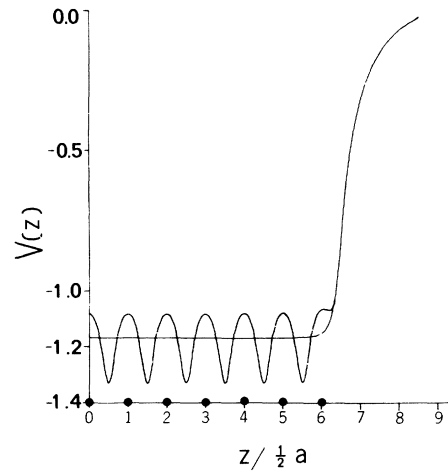


FIG. 3. Jellium potential and $V(\bar{G}=0, z)$, the planar averaged potential, for the 13-layer aluminum film.

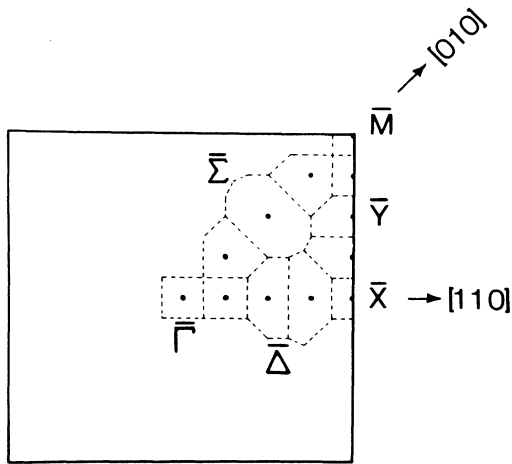


FIG. 5. Area associated with each point in the two-dimensional Brillouin zone at which calculations were made.

part to the difference between nonperturbative and perturbative calculations and in part due to the fact that we chose our pseudopotential to have an average value in the interior of the film equal to the jellium value, whereas Lang and Kohn considered the perturbative effect of a non-zero-average pseudopotential on the jellium result. Lang and Kohn's¹⁵ assumption that the polycrystalline work function is an average of the (001), (011), and (111) face work functions leads to an estimate of the true (001) work function being 0.2-eV larger than the polycrystalline experimental value of 4.19 eV.¹⁶

In Fig. 6 we show $\rho(\bar{\Gamma}, z)$ for six different values of $\bar{\Gamma}$. This was obtained by summing the squares of the absolute value of the pseudo-wave-functions with eigenvalues below the Fermi energy and weighting the contributions from the wave functions at each Brillouin zone point shown in Fig. 5 by the area surrounding that point. The boundaries of these areas are formed by the bisectors of lines joining the point at the center of the area to the other points. We note that near the center of our film the valence charge density varies from a maximum in the interstitial region of 3.76 electrons per atom to the minimum at atomic sites of 1.27. This is quantitatively different from the results of a recent bulk calculation by Walter, Fong, and Cohen.⁷ Although they found their maxima and minima at the same places as ours, their $\rho(\bar{\Gamma})$ varies only between 3.4 and 1.65 electrons per atom. We think that this results from their having taken all Fourier transforms of the potential other than V_{111} and V_{200} to be zero. Our potential has non-zero $V(k)$ for $k > |(2, 0, 0)|$ and thus, in real space, a more repulsive core region. Wider variations in charge density follow. In Fig. 7 we compare

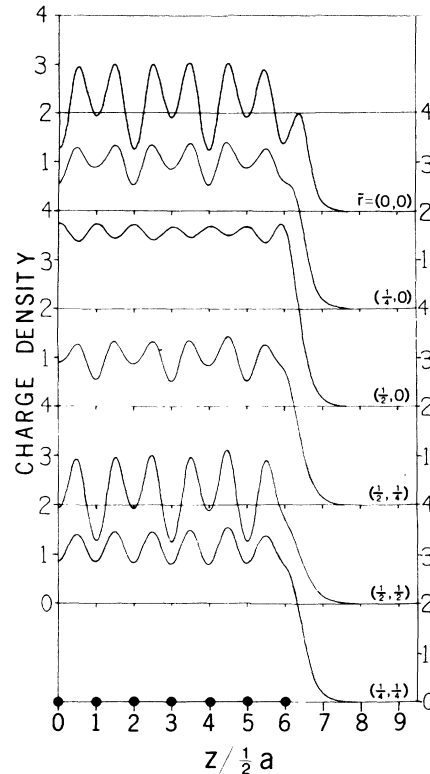


FIG. 6. Charge density $\rho(\bar{\Gamma}, z)$ (in units of e^- per atom) for six different planar positions, $\bar{\Gamma}$.

the jellium charge density with the planar average of our charge density which is obtained by Fourier transforming $\rho(\bar{\Gamma}=0, k_z)$. The similarity of these charge densities should not be surprising since our $V_{111m}(0, z)$ is so closely related to the jellium potential.

In Fig. 4 we have denoted surface states at $\bar{\Gamma}$, \bar{M} , and \bar{X} by S. It is interesting to note that the

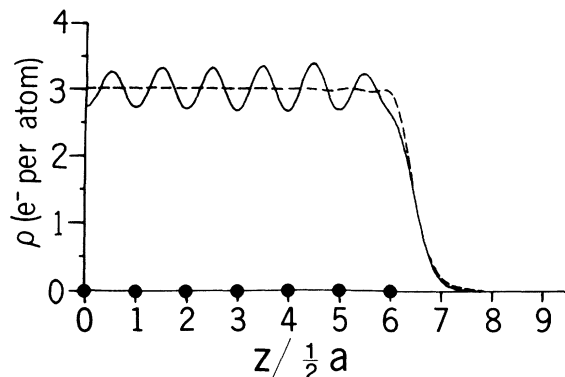


FIG. 7. Comparison of $\rho(\bar{\Gamma}=0, z)$, the planar average of the charge density with the jellium $\rho(z)$ from Ref. 6.

$\bar{\Gamma}_1^+$ surface state belongs to the same band as the lowest \bar{X}_3^+ surface state whereas the $\bar{\Gamma}_1^+$ and \bar{X}_3^+ states belong to bands which run out of the gap and into the continuum. Of course, the $\bar{\Delta}_1^+$ band to which $\bar{\Gamma}_1^+$ and \bar{X}_3^+ belong is a surface band only in the region of $\bar{\Gamma}$ and \bar{X} . The $\bar{\Gamma}_1^+$ surface states can be followed along $\bar{\Sigma}_1^+$ slightly past the point where they are crossed by $\bar{\Sigma}_2^+$ bands, i. e., into a region corresponding to the horizontally shaded region in Fig. 2. The \bar{M}_4^+ surface states appear in what would be a continuum of \bar{M}_5 states in a semi-infinite crystal and become surface resonances rather than localized surface states as soon as one moves away from \bar{M} by an infinitesimal distance in \bar{k} space.

Because the high-symmetry points require fewer S2DPW's, we were able to use more k_x 's in the expansion, allowing us to do the calculation for thicker films. In Fig. 8 we plot the $\bar{\Gamma}_1^+$ and \bar{M}_1^+ surface states for fixed \bar{r} as a function of z (Because of the translational relationship between \bar{M}_1 and \bar{M}_4 previously discussed, the \bar{M} surface states have \bar{M}_4 symmetry when the surface plane is an A plane and \bar{M}_1 symmetry when it is a B plane where the center plane of the film is an A plane). Because both wave functions are normalized and \bar{M}_1^+ has nodes at $\bar{r} = (\frac{1}{2}, \frac{1}{2})$ and $(\frac{1}{2}, 0)$ whereas $\bar{\Gamma}_1^+$ has no planar nodes, the \bar{M}_1^+ function is larger than the $\bar{\Gamma}_1^+$ at its antinodal \bar{r} points. Because of the large kinetic energy represented by its planar nodes, the \bar{M}_1^+ state has less kinetic energy to spend on z nodes than the $\bar{\Gamma}_1^+$ state. Hence the \bar{M}_1^+ function has a longer wavelength than the $\bar{\Gamma}_1^+$ function in Fig. 8. In Fig. 4 note that in the lower \bar{X}

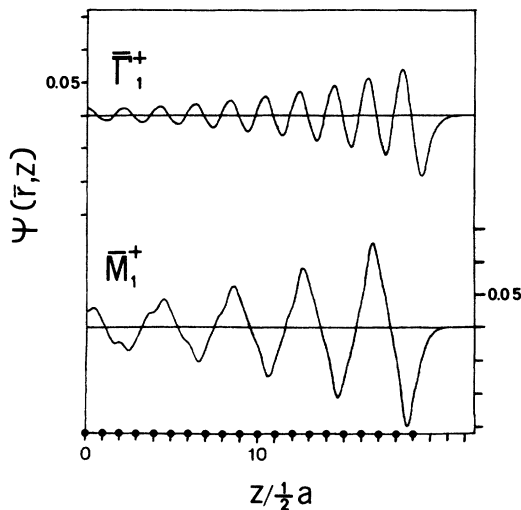


FIG. 8. Wave functions for surface states at $\bar{\Gamma}$ and \bar{M} calculated for a 39-layer Al film. $\bar{\Gamma}_1^+$ is plotted for $\bar{r} = (\frac{1}{2}, \frac{1}{2})$ and \bar{M}_1^+ for $\bar{r} = (0, 0)$.

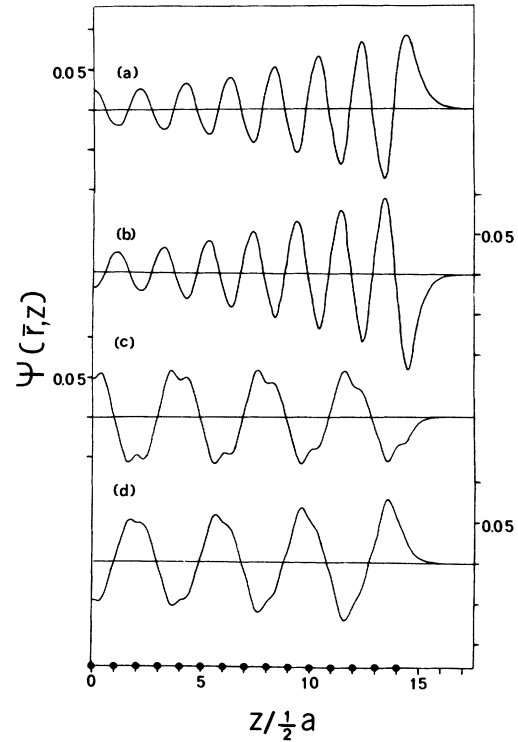


FIG. 9. Wave functions at \bar{X} calculated for a 29-layer Al film. (a) \bar{X}_3^+ surface state in the upper gap with $\bar{r} = (\frac{1}{2}, \frac{1}{2})$. (b) \bar{X}_1^+ surface state in the upper gap with $\bar{r} = (\frac{1}{2}, \frac{1}{2})$. (c) \bar{X}_1^+ nonsurface state which forms the upper edge of the lower gap with $\bar{r} = (0, 0)$. (d) \bar{X}_3^+ surface state in the lower gap with $\bar{r} = (\frac{1}{2}, \frac{1}{2})$.

gap there are \bar{X}_3^+ surface states but in the upper \bar{X} gap there are both \bar{X}_3^+ and \bar{X}_1^+ surface states. In Fig. 9 we plot the three (+) symmetry surface states along with the \bar{X}_1^+ bulk state which forms the upper edge of the lower gap for a 29-layer film. In Table II we list decay constants for these surface states determined by passing straight lines through the peaks of the curves drawn on semilog paper. Even for simple discontinuous model potentials the decay constant is a rather complicated function of the potential.¹⁷ In general, however, the wider the gap, the larger the decay constant. Note that the widths of the various gaps are approximately $2V_{200}$ for $\bar{\Gamma}$ and upper \bar{X} , $4V_{111}$ for \bar{M} , and $2V_{111}$ for lower \bar{X} and that the decay constants are consistent with these relative widths.

We also see in Figs. 8 and 9 that the surface states have not decayed completely to zero, even at the center of a 29- or 39-layer film. For this reason, surface states on the two opposite faces interact. In an infinitely thick film the surfaces would have the same energy and even and odd symmetry combinations would be degenerate. But as we see in Fig. 4, the overlap has split this natural

TABLE II. Decay constants in inverse Bohr radii for surface states at high-symmetry points. Eigenvalues are given in rydbergs. The first two eigenfunctions were computed for a 39-layer film with six selvage layers, and the last three eigenfunctions were calculated for a 29-layer film with six selvage layers.

Wave function	Eigenvalue	Decay constant	$\bar{\Gamma}$
$\bar{\Gamma}_1^+$	-0.5307	0.027 ± 0.001	$(\frac{1}{2}, 0)$
\bar{M}_1^+	-0.3001	0.023 ± 0.0005	$(0, 0)$
\bar{X}_3^+	-0.1841	0.0275 ± 0.001	$(\frac{1}{2}, 0)$
\bar{X}_1^+	-0.2088	0.031 ± 0.002	$(0, 0)$
\bar{X}_3^+	-0.6766	0.007 ± 0.002	$(\frac{1}{2}, 0)$

degeneracy of the surface states. This is another effect of film thickness, and as we go from a 13-layer film to a 39-layer film the splitting of the surface states at $\bar{\Gamma}$ and \bar{M} changes from 0.042 and 0.029 Ry, respectively, to 0.002 and 0.002 Ry. As we go from a 13- to 29-layer film the splitting of the states in the lower \bar{X} gap goes from 0.039

to 0.013 Ry. The splittings of the states in the upper gap goes from 0.045 to 0.007 Ry and from 0.044 to 0.009 Ry.

In conclusion, we find surface states on the (001) surface of aluminum. These are of various types; some of them are occupied and some will be above the Fermi surface. We find surface states at \bar{X} which were not reported by Boudreaux, and we find that they extend along both the $\bar{\Delta}$ and \bar{Y} directions. We find that the energy gap along the $\bar{\Sigma}$ direction disappears before reaching \bar{M} , and we do not find the surface state extending along $\bar{\Sigma}$ from \bar{M} which Boudreaux reported. In addition, we have found that comparing our 13-layer results to results at special points for thicker films and to a two-dimensional projection of the three-dimensional infinite-crystal energy bands elucidates the effects of the surface.

Note added in proof. Dr. Boudreaux has reviewed his calculation and concludes that he properly included all points in the three-dimensional Brillouin zone.

*Research sponsored by the Air Force Office of Scientific Research (AFSC) under Grant No. AF-AFOSR-72-2308 and by the National Science Foundation under Grant No. GH-40371.

¹G. P. Alldredge and L. Kleinman, Phys. Rev. Lett. **28**, 1264 (1972).

²D. S. Boudreaux, Surf. Sci. **28**, 344 (1971).

³R. E. Allen, G. P. Alldredge, and F. W. de Wette, Phys. Rev. B **4**, 1661 (1971).

⁴A. O. E. Animalu and V. Heine, Philos. Mag. **12**, 1249 (1965); W. A. Harrison, *Pseudopotentials in the Theory of Metals* (Benjamin, New York, 1966).

⁵N. W. Ashcroft, Philos. Mag. **8**, 2055 (1963).

⁶N. D. Lang and W. Kohn, Phys. Rev. B **1**, 4555 (1970).

⁷J. P. Walter, C. Y. Fong, and M. L. Cohen, Solid State Commun. **12**, 303 (1973).

⁸For $\zeta = 0.5$, $1 - \zeta$ is identical to ζ and is not counted for exactly the same reason that states on opposite faces of Brillouin zones are not both counted.

⁹That this is the case can be seen by considering the lowest symmetrized combinations of three-dimensional plane waves which project to \bar{M} in two dimensions. \bar{M}_1 and \bar{M}_4 are formed from a combination of $Z_1 = 2^{-1/2} \{(1, 0, 1/2 - \alpha) + (-1, 0, 1/2 - \alpha)\}$ and $Z_2 = 2^{-1/2} \{(0, 1, -1/2 - \alpha) + (0, -1, -1/2 - \alpha)\}$, whereas the \bar{M}_5 states are formed from $Z_3 = 2^{-1/2} \{(1, 0, 1/2 - \alpha) - (-1, 0, 1/2 - \alpha)\}$ and $Z_4 = 2^{-1/2} \{(0, 1, -1/2 - \alpha) - (0, -1, -1/2 - \alpha)\}$.

The secular determinants are thus

$$Z_{12} = \begin{pmatrix} (2\pi/a)^2 [1 + (\frac{1}{2} - \alpha)^2] + V_0 + V_{200} - E & 2V_{111} \\ 2V_{111} & (2\pi/a)^2 [1 - (\frac{1}{2} - \alpha)^2] - V_0 - V_{200} - E \end{pmatrix}.$$

$$Z_{34} = \begin{pmatrix} (2\pi/a)^2 [1 + (\frac{1}{2} - \alpha)^2] + V_0 - V_{200} - E & 0 \\ 0 & (2\pi/a)^2 [1 - (\frac{1}{2} + \alpha)^2] - V_0 - V_{200} - E \end{pmatrix}.$$

Solving the secular equations with $0 \leq \alpha \leq 1/2$, we find that \bar{M}_5 spans the energy range between $(2\pi/a)^2 + V_0 - V_{200}$ and $2(2\pi/a)^2 + V_0 - V_{200}$ and \bar{M}_1, \bar{M}_4 span the energy range between $(2\pi/a)^2 + V_0 + V_{200}$ and $2(2\pi/a)^2 + V_0 + V_{200}$ but with a gap of width $4V_{111}$ centered at $E = 1.25(2\pi/a)^2 + V_0 + V_{200}$.

¹⁰Points in the extended three-dimensional Brillouin zone (B.Z.) commensurate with the square B.Z. lying outside the primitive B.Z. can be translated back into the primitive B.Z. which changes the planar projection \bar{k} .

¹¹V. Heine, Proc. Phys. Soc. Lond. **81**, 300 (1963).

¹²G. P. Alldredge and L. Kleinman (unpublished).

¹³For (001) films we always take an odd number of layers so that the film will have z -reflection symmetry and the even and odd basis functions will not mix.

¹⁴This very surprising result, that the bottom of the thin-film conduction bands is lower than the bottom of the bulk bands when the same V_0 is used to calculate both, can be understood as follows. Consider the difference between the bulk potential and the potential of a succession of thin films (i.e., 13 occupied layers, 6 missing layers, 13 occupied, ect.) as a perturbation. Now if its off-diagonal effect is larger than its diagonal effect, it will lower the lowest eigenvalue. Note that one may not take the opposite point of view that the negative of this potential is a perturbation on the thin-film bands for the reason that the infinite-crystal eigenfunctions form a complete set for a succession of thin films but the eigenfunctions of a succession of thin films lack the proper periodicity to be a complete set for the infinite crystal.

¹⁵N. D. Lang and W. Kohn, Phys. Rev. B **3**, 1215 (1971).

¹⁶J. C. Riviere, in *Solid State Surface Science*, edited by M. Green (Marcel Dekker, New York, 1969), Vol. I.

¹⁷L. Kleinman, Phys. Rev. B **6**, 1142 (1972).